

Low temperature microwave sintering of yttrium and samarium co-doped ceria solid electrolytes for IT-SOFCs

Kasarapu Venkataramana¹ · K. Ravindranath^{1,2} · Chittimadula Madhuri¹ · Ch Madhusudan¹ · N. Pavan Kumar³ · C. Vishnuvardhan Reddy¹

Received: 7 May 2017 / Revised: 5 July 2017 / Accepted: 27 September 2017 / Published online: 12 October 2017
© Springer-Verlag GmbH Germany 2017

Abstract Nanocrystalline co-doped ceria $\text{Ce}_{0.8}\text{Sm}_{0.2-x}\text{Y}_x\text{O}_{2-\delta}$ solid electrolytes for intermediate-temperature solid oxide fuel cells (IT-SOFCs) were synthesized through sol–gel auto-combustion method. The prepared samples were sintered via microwave sintering at 1200 °C for 1 h. The X-ray diffraction analysis of co-doped ceria system reveals formation of the samples with a single-phase cubic fluorite structure. The lattice parameter values were calculated from X-ray diffraction patterns. The calculated crystallite sizes of all the samples were found to be in the range of 17 and 28 nm. Surface morphologies and elemental analysis of all the samples were carried out by using SEM and EDS analysis. The existence of chemical bonding in the samples was studied by FTIR spectroscopy. The presence of oxygen vacancies and evaluation of their concentration in the material was carried out using Raman spectroscopy analysis. Electrical properties of all the

samples were analyzed by impedance spectroscopy. It was found that microwave sintered co-doped ceria sample $\text{Ce}_{0.8}\text{Sm}_{0.1}\text{Y}_{0.1}\text{O}_{2-\delta}$ exhibits the highest total ionic conductivity with minimum activation energy among all the compositions and conventional sintered sample. Therefore, it can be concluded that the microwave sintered $\text{Ce}_{0.8}\text{Sm}_{0.1}\text{Y}_{0.1}\text{O}_{2-\delta}$ sample may be useful as a promising electrolyte material for the IT-SOFCs.

Keywords Co-doped ceria · Solid electrolyte · Raman · Total ionic conductivity · IT-SOFCs

Introduction

Solid oxide fuel cells (SOFCs) have emerged as potential electrochemical devices for efficient alternate energy resources and have the capacity to provide clean electricity with high efficiency and low environmental impact [1, 2]. The solid electrolyte material is one of the important components among all the components of SOFC. A best solid electrolyte must require high ionic, low electronic conductivity and high stability for different reducing and oxidizing atmospheres. Ytria-stabilized zirconium (YSZ) and cerium oxides are the two major and important electrolyte materials for the application of SOFCs. The traditional YSZ is a well-known electrolyte material in SOFC, but it requires a high temperature (> 700 °C) to exhibit the high ionic conductivity [3]. This high operating temperature (> 700 °C) of SOFC may result in material degradation and thermal mismatch between the adjacent electrolyte and electrode components, which leads to a decrease in the lifetime of SOFC system [4]. Cerium oxide as a solid electrolyte was thoroughly investigated so far, which exhibits the superior ionic conductivity over traditional YSZ (8 mol% of Y, YSZ) in the intermediate temperature range,

Highlights • The system $\text{Ce}_{0.8}\text{Sm}_{0.2-x}\text{Y}_x\text{O}_{2-\delta}$ has been synthesized via sol–gel auto-combustion method followed by microwave sintering.

- The comparison of microwave and conventional sintering has been made.
- Influence of oxygen vacancy concentration on total ionic conductivity is investigated.
- Thermal expansion coefficient of $\text{Ce}_{0.8}\text{Sm}_{0.1}\text{Y}_{0.1}\text{O}_{2-\delta}$ is studied and compared.
- Highest total ionic conductivity of microwave sintered $\text{Ce}_{0.8}\text{Sm}_{0.1}\text{Y}_{0.1}\text{O}_{2-\delta}$ sample makes it use as a potential electrolyte for IT-SOFCs.

✉ C. Vishnuvardhan Reddy
kvrugoud56@gmail.com

- ¹ Department of Physics, Osmania University, Hyderabad 500007, India
- ² Indian Institute of Chemical Technology, Hyderabad 500007, India
- ³ Advanced Magnetics Group, Defence Metallurgical Research Laboratory, Hyderabad 500058, India

i.e., in between 400 and 600 °C [4–7]. The ionic conductivity of ceria is significantly increased by doping with rare earth cations and the materials such as $\text{Ce}_{0.8}\text{Gd}_{0.2}\text{O}_2$, $\text{Ce}_{0.8}\text{Y}_{0.2}\text{O}_2$, $\text{Ce}_{0.8}\text{La}_{0.2}\text{O}_2$, $\text{Ce}_{0.8}\text{Nd}_{0.2}\text{O}_2$, and $\text{Ce}_{0.8}\text{Sm}_{0.2}\text{O}_2$ have been investigated and reported [7]. Among the various doped ceria materials, $\text{Ce}_{0.8}\text{Sm}_{0.2}\text{O}_2$ shows the superior properties like high ionic conductivity and low activation energy. However, the single doped ceria is not a good conductor due to (1) the increase in electronic conductivity along with ionic conductivity, (2) less energy conversion efficiency under minimum oxygen partial pressures, and (3) the cerium being reduced from + 4 state to + 3 state [8–11]. Pikalova et al. [8] reported that the critical partial pressure values of oxygen in the double doped ceria system were higher than that of single doped ceria system. Therefore, ceria-based electrolytes require the structural modification (i.e., creation of oxygen vacancies) to preserve the charge balance. The oxygen vacancies were significantly increased by co-doping in ceria, which results in the enhanced electrical properties compared to single doped ceria [8, 11].

Apart from dopants, the preparation method, sintering temperature, and time can also influence the performance of co-doped ceria electrolyte materials. Earlier, Dudek et al. [12–14], Cheng et al. [15], and Sha et al. [16] have reported on $\text{CeO}_2\text{–Sm}_2\text{O}_3\text{–Y}_2\text{O}_3$ system with different synthesis techniques (i.e., co-precipitation, hydrothermal, gel casting, and sol–gel method) and approach the sintering temperature in between 1300 and 1600 °C in order to investigate the microstructure and the mechanical, thermal, and electrical properties. It was found that the performance of a ceria-based electrolyte material may also depend upon the preparation technique. Among the most commonly used techniques, sol–gel auto-combustion method is better due to the smaller particle size and improved purity and homogeneity of a material [11]. However, no systematic investigations have been made to achieve the enhanced properties of yttrium and samarium co-doped ceria-based system by reducing the sintering temperature and time [17, 18]. In the last few years, the process of microwave sintering has an enormous demand for the ceramic materials technology in which microwave energy is used for sintering the materials in place of the conventional sintering. The microwave sintering is a microscopic-level rapid heating and it requires less consumption of energy and time when compared to conventional sintering. Recently, researchers are inclined to approach the microwave sintering using microwave energy in order to achieve enhanced properties of a ceria-based material [17–20].

In this paper, we reported the structural, electrical, and thermal properties of microwave-sintered co-doped ceria $\text{Ce}_{0.8}\text{Sm}_{0.2-x}\text{Y}_x\text{O}_{2-\delta}$ system using sol–gel auto-combustion method. A comparison is made with $\text{Ce}_{0.8}\text{Sm}_{0.1}\text{Y}_{0.1}\text{O}_{2-\delta}$ sample sintered using conventional sintering method to understand the advantage of microwave sintering over conventional sintering.

Experimental

The nanocrystalline co-doped ceria $\text{Ce}_{0.8}\text{Sm}_{0.2-x}\text{Y}_x\text{O}_{2-\delta}$ (CSY) ($x = 0.0, 0.05, 0.10, 0.15,$ and 0.20 , named as CSY0, CSY5, CSY10, CSY15, and CSY20) materials were synthesized by sol–gel auto-combustion synthesis [11]. Ceric ammonium nitrate, samarium nitrate and yttrium nitrate, citric acid, and ammonia solutions were used as initial materials. The resultant powder was grounded to get a fine homogeneous powder and calcined at 800 °C for 2 h. The calcined powders were then pressed into circular pellets with 10 mm diameter and ≥ 2 mm thickness by hydraulic press operated at a pressure of 5 tons per square inch. The pressed pellets were then sintered by microwave energy with a 2.45 GHz furnace in order to obtain the dense co-doped ceria ceramics. Microwave sintering was carried out at 1200 °C for 1 h soaking time, with heating and cooling, at a rate of 20°C/min. For comparison, the prepared pellet of CSY10 was also sintered by conventional sintering in air atmosphere using muffle furnace at 1300 °C for 4 h with heating and cooling at a rate of 5 °C/min and nomenclature given as CSY10C.

The powder X-ray diffraction patterns of the samples were recorded using a Philips X-pert PRO ALPHA1 analytical diffractometer. The microstructure and elemental composition of the samples were performed by scanning electron microscope with energy-dispersive spectrum using ZEISS EVO. The functional groups and chemical bonding were obtained by an FTIR spectrometer using SHIMAZ MAKE FTIR 8400. The sample formation and vibration modes of samples were carried out using Horiba-Jobin Yvon micro-Raman spectrometer. Wayne Kerr impedance analyzer 6500B was used to carry out impedance measurements of the co-doped ceria samples. The linear thermal expansion measurements were done by using a DIL 402 PC dilatometer.

Results and discussion

XRD analysis

Figure 1 represents the powder X-ray diffraction (PXRD) patterns of microwave-sintered co-doped ceria samples including the conventional sintered CSY10C sample. The PXRD patterns confirm the presence of single phase in all the compositions with a cubic fluorite structure of space group $\text{Fm}\bar{3}\text{m}$ (JCPDS powder diffraction File No. 34-0394) and no other phase was observed. Fullprof software is used to refine the XRD analysis of CSY10 and the Reitveld refinement of this sample is shown in Fig. 2. It can be seen from the figure that the difference between the observed and calculated XRD data was almost a straight line indicating the accuracy of the fitting and the goodness-of-fit value is in between 1 and 2 [4]. The

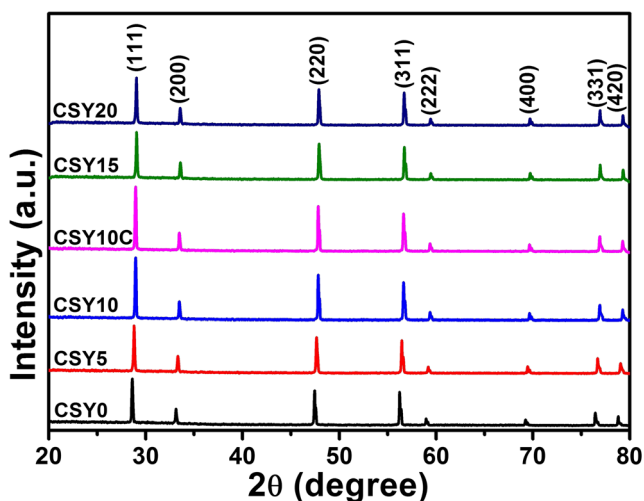


Fig. 1 XRD patterns of CSY system

lattice parameter (a) values were calculated from the PXRD patterns and were found to decrease linearly from 5.4387 to 5.4187 Å with increasing Y^{3+} concentration due to the smaller ionic radius of Y^{3+} (1.159 Å) compared to Sm^{3+} (1.219 Å) [21]. Scherer formula was used to calculate the crystallite size of all the co-doped ceria samples, which is measured from the full-width half maxima of (111) peak by the following equation [22]:

$$D = \frac{K\lambda}{\beta \cos\theta} \quad (1)$$

Where K (= 0.90) is shape factor, λ (= 1.5406 Å) is the wavelength of the radiation, θ is the diffraction angle, β is the full-width half maxima (in radians), and D is the crystalline size. The calculated crystallite sizes of the CSY samples were found in between 17 and 28 nm. Relative densities of all the sintered specimens were calculated from the measured density (D_m , using Archimedes principle) and theoretical density (D_{th}) and were found to be above 94%. The highest value of relative density was observed for CSY10 which is higher than CSY10C. Table 1 represents the crystallographic data (i.e., crystal structure, lattice parameter, volume, relative density, and crystallite size) of CSY system.

SEM analysis

Scanning electron microscope (SEM) of a material plays a vast role in the analysis of structural properties. Figure 3 depicts the SEM images of microwave-sintered specimens of co-doped ceria system and conventional sintered CSY10C sample. It can be observed from Fig. 3 that the grains were well distributed in cluster form. It can also be observed that all the sintered CSY specimens were dense in microstructure with

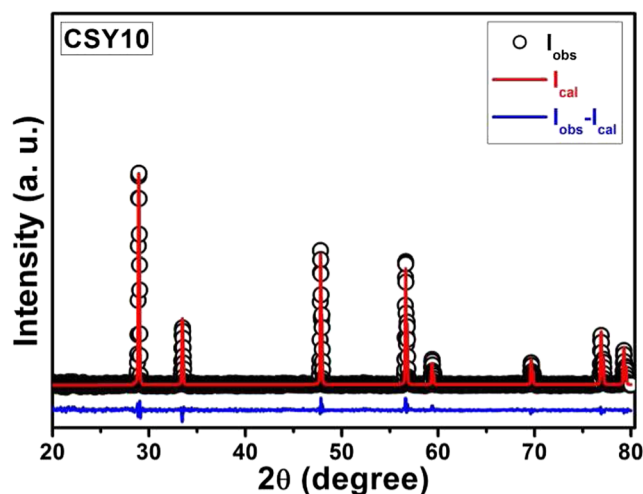


Fig. 2 Reitveld refinement for $Ce_{0.8}S_{0.1}Y_{0.1}O_{2-\delta}$ (CSY10) sample

spherical shape. The average grain sizes of entire CSY samples were calculated from the SEM images and were found to be in the range of 293–465 nm. Figure 4 represents the EDS analysis of co-doped ceria system, which confirms the presence of Ce, Sm, Y, and O elements in the samples. Elemental composition analysis of all the samples is listed in Table 2.

FTIR analysis

The vibrations of the functional derivatives in co-doped ceria samples have been investigated using FTIR spectroscopy. FTIR is used to obtain additional information on the phase and structure transformation of cerium oxide phases over XRD analysis [25]. The FTIR spectra of co-doped ceria electrolyte samples are shown in Fig. 5. It shows that there are few bands in the range from 400 to 4000 cm^{-1} and the bands were attributed to the various functional groups. Among the absorption bands, a broad band at 3433 cm^{-1} is due to the characteristic of adsorbed water due to moisture (O–H stretching) [11, 23]. The low intense absorption bands at 2926 cm^{-1} , 2854 cm^{-1} corresponds to C–H stretching vibration. The low intense peak at 2373 cm^{-1} is attributed to –N–H stretching vibration due to unwanted carbonates in the material [23–25] and 1747 cm^{-1} is related to C=O stretching mode [26]. The strong absorption band appears at 1634 cm^{-1} and is attributed to bending overtone of O–H and peak at 1458 cm^{-1} corresponds to H–C–H bending vibration band [27]. Small peak at 1163 cm^{-1} and intense band appears at 1044 cm^{-1} was due to stretching vibration mode of Ce–O group or CH–OH stretching vibration. The absorptions in between 876 and 463 cm^{-1} represent the characteristic cerium–oxygen vibration band, which confirms the material formation of yttrium and samarium co-doped ceria system [23–27]. FTIR analysis reveals the presence of functional groups and chemical bonding in the co-doped ceria compositions confirms the formation

Table 1 Crystallographic data of CSY system

Sample ID	Crystal structure	Lattice parameter (Å)	Volume (Å ³)	Relative density (%)	Crystallite size (<i>D</i>) (nm)
CSY0	Cubic	5.4387	160.87	94.8	17
CSY5	Cubic	5.4338	160.44	95.3	19
CSY10	Cubic	5.4289	160.01	96.2	21
CSY15	Cubic	5.4241	160.17	95.8	25
CSY20	Cubic	5.4187	159.11	95.6	28
CSY10C	Cubic	5.4294	160.05	96.1	22

of samples with cubic fluorite structure as evidenced by the XRD analysis [11].

Raman analysis

Raman spectroscopy is a vital study to investigate the purity, quality, and structural analysis of the electrolyte materials. Raman spectroscopy analysis reveals the presence of oxygen vacancies and evaluation of their concentration in the material [28–31]. The Raman spectra of these co-doped ceria samples are shown in Fig. 6. The spectrum of pure CeO₂ shows one

Raman allowed band with frequency centered around 460 cm⁻¹, which is the characteristic of symmetric F_{2g} Raman active mode of the fluorite-like CeO₂ structure, and it is assigned to the symmetric vibration of the oxygen atoms around the cerium ions [29]. The additional Raman peak around 570 cm⁻¹ is attributed to the intrinsic oxygen vacancies (defect spaces include O²⁻ vacancies). This relatively weak intensity mode results from the presence of few intrinsic oxygen vacancies in the cerium lattice which is maintaining the charge neutrality in the crystal lattice when Ce⁴⁺ ions were replaced by samarium and yttrium ions. This is due to the non-stoichiometry of nanocrystalline Y³⁺ and Sm³⁺ co-doped ceria powders [11, 30]. It can be observed from Fig. 6 that the intensity ratio (i.e., I_{570}/I_{460}) slightly increases with increasing Y³⁺ content up to 10 mol%, i.e., CSY10, and then decreases.

The concentration of oxygen vacancies plays a key role in electrolyte materials' electrical properties. The Raman spectra which reveals the information about concentration of structural oxygen vacancies were calculated using full-width half maxima (FWHM) of 460 cm⁻¹ peak and area ratio of 570 cm⁻¹ and 460 cm⁻¹ peaks [30, 31]. Table 3 shows the FWHM₄₆₀ and area ratio (A_{570}/A_{460}) of CSY system of samples. It can be seen from the table that the CSY10 sample is found to have higher values of FWHM, intensity ratio as well as area ratios compared to all samples and also conventional

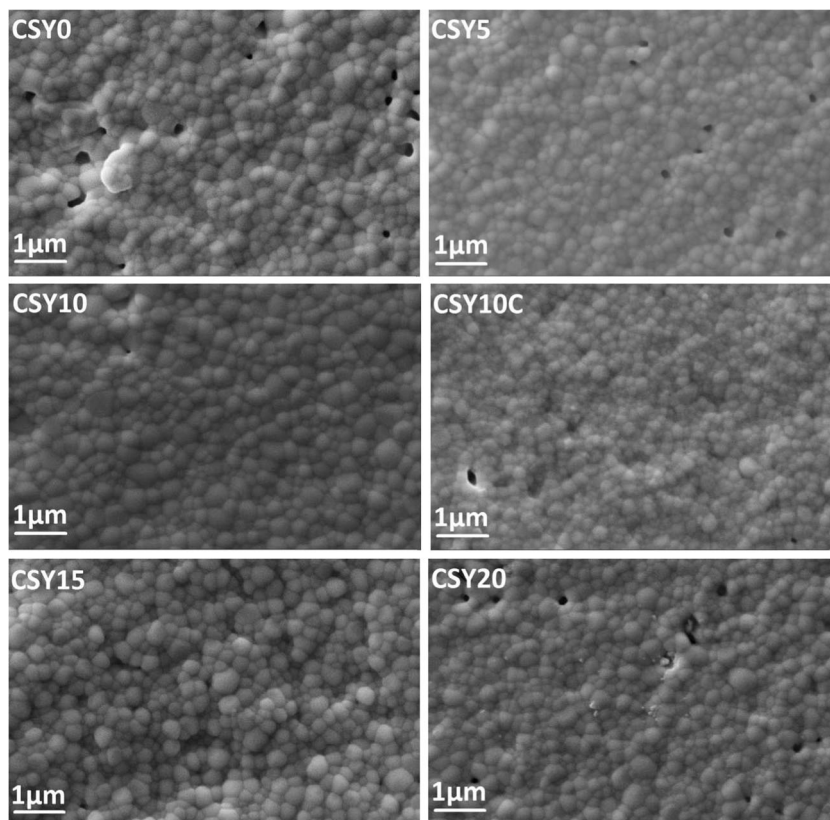
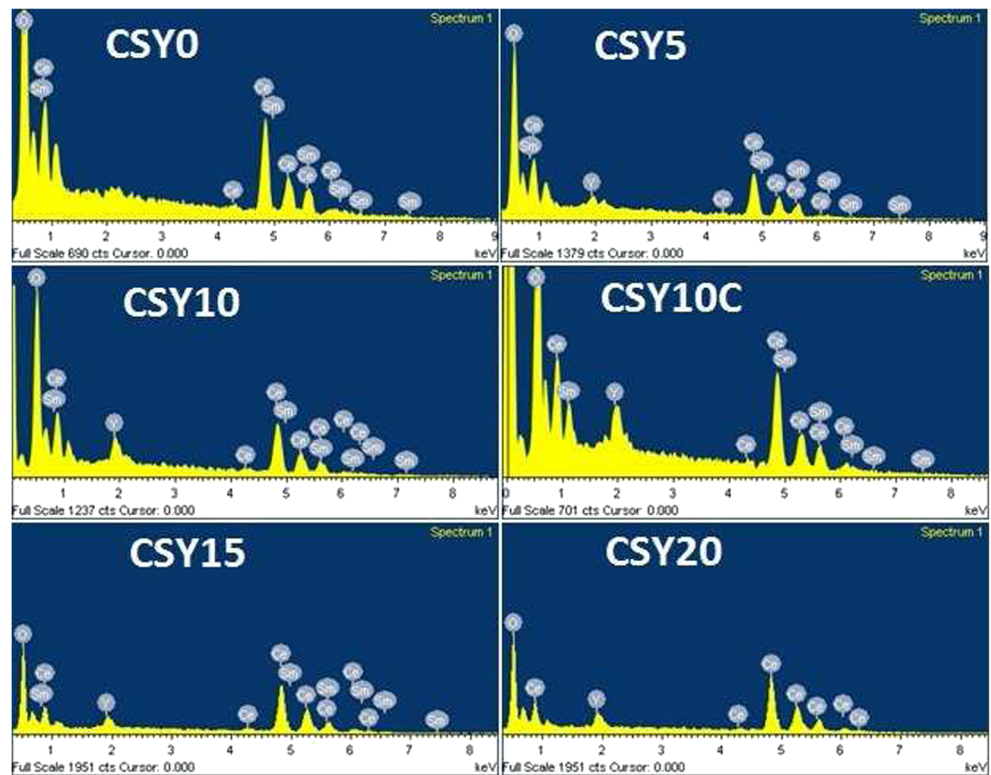
Fig. 3 SEM images of CSY system

Fig. 4 EDS analysis of CSY system



sintered CSY10C sample which indicates high concentrated oxygen vacancies in CSY10. Therefore, one can expect the higher total ionic conductivity and small activation energies for the CSY10 sample [30, 31].

Electrical properties

Impedance spectroscopy is an important tool to understand the electrical conductivity behavior of solid electrolyte material in solid oxide fuel cell applications [31–34]. In the present investigation, the impedance spectrum of sintered CSY system was recorded in the temperature range from 250 to 600 °C and in the frequency range from 100 Hz to 5 MHz. Figure 7

depicts the complex impedance plots [i.e., Nyquist plots of real part (Z') and imaginary part (Z'') of impedance] for all the co-doped ceria samples at 500 °C. Complex impedance plots at 500 °C of all the specimens were fitted by Z-View software using a series of resistor (R) and constant phase elements (CPE) connected in parallel as shown in Fig. 7. The constant phase element was used to fit the impedance plots in place of simple capacitor because some depression of arcs occurs in the electrical response of the material [4, 31].

Table 2 Elemental composition analysis (EDS) of CSY system

Sample	Atomic percentage of elements			
	Ce	Sm	Y	O
CSY0	26.42	6.81	–	66.77
CSY5	26.16	5.21	1.08	67.55
CSY10	26.91	3.39	3.34	66.36
CSY15	26.48	1.91	5.04	66.57
CSY20	27.01	–	6.31	66.68
CSY10C	26.81	3.40	3.37	66.42

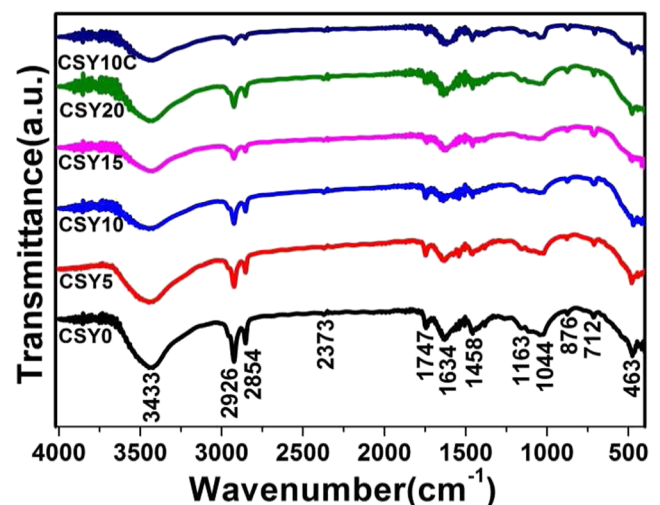


Fig. 5 FTIR spectra of CSY system

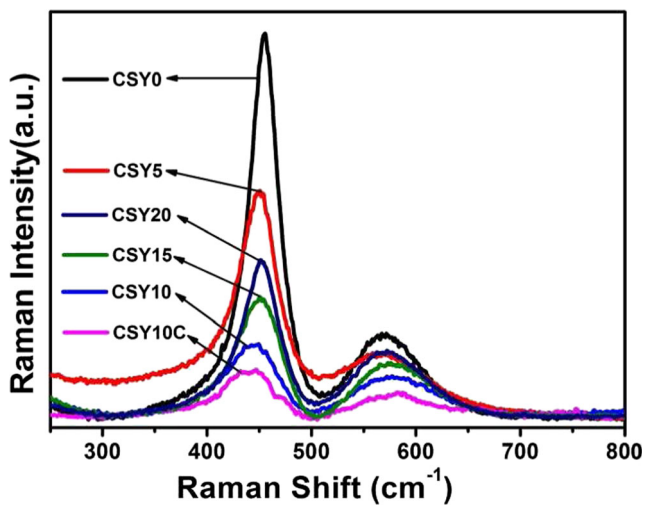


Fig. 6 Raman spectra of CSY system

Table 4 represents the fitted results of the complex impedance plots for CSY system. The behavior of complex impedance plot is a characteristic conducting nature of the specimen [32]. It can be observed from Fig. 7 that the semi-circle starts at lower frequency on the Z' axis and the curve area under the semi-circle tends to decrease with the increase in dopant concentration up to 10 mol% of yttrium, i.e., CSY10, indicating the increase in conductivity of the specimen. Total resistance (R_t), which is the sum of the grain and grain boundary resistance, was calculated in order to obtain the total ionic conductivity of the specimens. The total ionic conductivity (σ_t) is calculated using the formula

$$\sigma_t = \frac{l}{R_t A} \quad (2)$$

where R_t is the total resistance, l is the thickness of the specimen, and A is the collect electrode area. The total ionic conductivity is found to increase with increasing dopant level (up to 10 mol%) as well as the temperature and CSY10 exhibits the highest total ionic conductivity, i.e., 2.5×10^{-2} S/cm at 600 °C whereas CSY10C exhibits 1.7×10^{-2} S/cm at the same temperature. The highest total ionic conductivity of

Table 3 Raman analysis for CSY system

Sample	FWHM ₍₄₆₀₎	I_{570}/I_{460}	A_{570}/A_{460}
CSY0	34	0.20	0.37
CSY5	39	0.31	0.49
CSY10	50	0.69	0.92
CSY15	46	0.51	0.62
CSY20	42	0.42	0.55
CSY10C	49	0.55	0.79

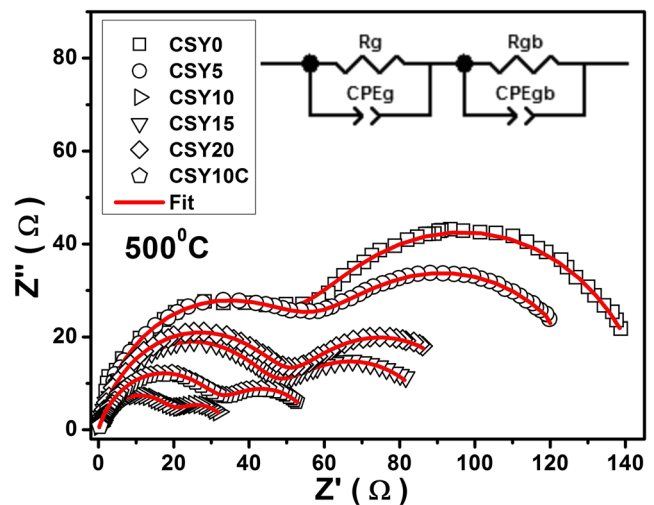


Fig. 7 Complex impedance plots at 500 °C of CSY system

microwave-sintered CSY10 sample over conventional sintered CSY10 is evidenced by the relative density and oxygen vacancy concentration from the above microstructure and Raman analysis (Tables 1 and 3). Figure 8 illustrates the grain, grain boundary, and total ionic conductivity versus temperature inverse for all the CSY specimens. It can be observed from Fig. 8 that there is a change in total conductivity which resulted in change of slope at/above 400 °C. This change may be attributed to the presence of different activation energies in the compositions, like association energy (due to vacancy associated with the cation trapping) and migration energy (due to free migration of oxygen vacancies in the lattice). At low temperatures (≤ 400 °C), the activation energy results in sum of the association and migration energies and at/above 400 °C, and only migration energy gives the activation energy due to the more number of free migrated oxygen vacancies [4, 34]. The calculated grain, grain boundary, and total ionic conductivity values at 500 °C and total ionic conductivity at 600 °C for all the CSY specimens are listed in Tables 4 and 5. The formation of concentrated mobile oxygen vacancies are responsible for the highest total ionic conductivity, which is evident by Raman analysis [4, 30, 31]. The total ionic conductivity values of microwave-sintered sample CSY10, conventional sintered sample CSY10C, and doped ceria samples reported in literature are shown in Table 6. It is clear from Table 6 that the microwave-sintered sample CSY10 is found to have high value of total ionic conductivity compared to all the samples except the sample reported in Dudek et al. [12], which was conventionally sintered at very high temperature of 1500 °C. This clearly shows the improved properties of CSY10 co-doped ceria system sintered by microwave sintering at lower temperature compared with the samples sintered by conventional sintering at high temperatures. It can be seen from Fig. 7 that as composition increases, there is a large change in the grain boundary resistance compared to

Table 4 Fitting results of complex impedance plots for CSY system

Sample	Temperature (°C)	R_g (Ω)	CPE-T (F)	CPE-P	R_{gb} (Ω)	CPE-T (F)	CPE-P	R_t (Ω)	σ_t (S/cm)
CSY0	500	52	0.0007	0.92	96	0.009	0.89	148	2.7×10^{-3}
	600	–	–	–	–	–	–	52	7.7×10^{-3}
CSY5	500	56	0.00025	0.89	79	0.0041	0.85	129	3.1×10^{-3}
	600	–	–	–	–	–	–	45	8.3×10^{-3}
CSY10	500	20	0.00041	0.77	15	0.02	0.72	35	1.1×10^{-2}
	600	–	–	–	–	–	–	16	2.5×10^{-2}
CSY15	500	46	0.00012	0.84	45	0.0092	0.71	91	4.4×10^{-3}
	600	–	–	–	–	–	–	36	1.1×10^{-2}
CSY20	500	50	0.0018	0.85	53	0.078	0.79	103	3.9×10^{-3}
	600	–	–	–	–	–	–	40	9.8×10^{-3}
CSY10C	500	32	0.00053	0.79	26	0.03	0.71	58	6.9×10^{-3}
	600	–	–	–	–	–	–	23	1.7×10^{-2}

grain resistance; this is due to grain boundary blocking factor (α_{gb}). The grain boundary blocking factor (α_{gb}) for all the samples at 500 °C was calculated using below equation [33]:

$$\alpha_{gb} = \frac{R_{gb}}{R_g + R_{gb}} \tag{3}$$

where α_{gb} is the grain boundary blocking factor, R_g is the resistance of grain, and R_{gb} is resistance of grain boundary. The calculated grain boundary blocking factor values are listed in Table 5. The CSY10 sample shows the lowest value

of α_{gb} , i.e., 0.43, which is lower than CSY10C and has the highest value of total ionic conductivity [33].

The activation energy (E_a) for conduction is calculated from the temperature dependence of conductivity plots using Arrhenius relation.

$$\sigma T = \sigma_0 \exp\left(-\frac{E_a}{KT}\right) \tag{4}$$

where E_a is activation energy, σ_0 is the pre-exponential factor, K is a Boltzmann constant, and T is absolute temperature. The activation energy values for grain, grain boundary,

Fig. 8 Temperature dependence of grain (a), grain boundary (b), and total ionic conductivity (c) of CSY system

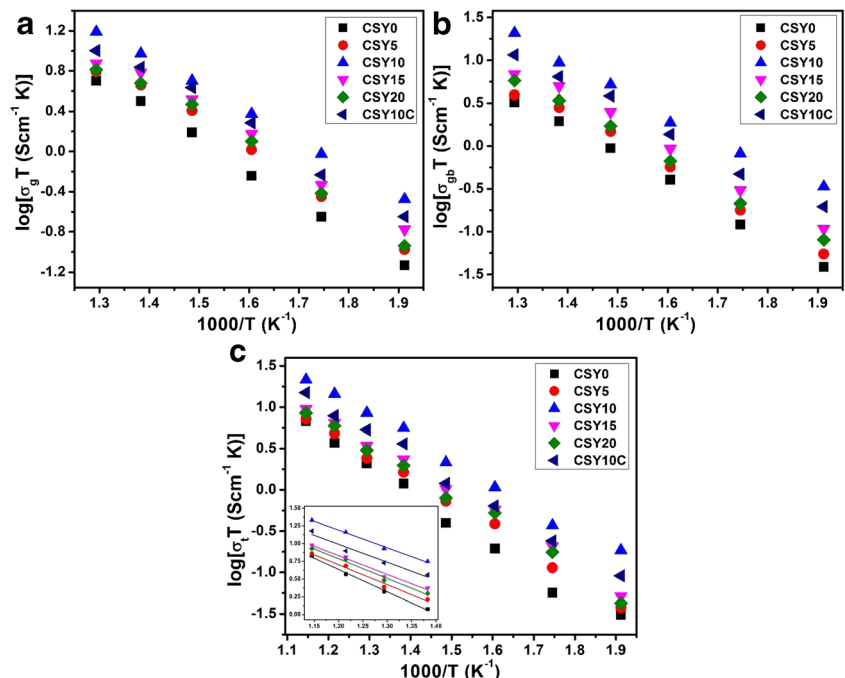


Table 5 Grain boundary blocking factor, conductivities, and activation energies corresponding to grain and grain boundaries at 500 °C for CSY system

Sample	α_{gb}	σ_t^g (S/cm)	σ_t^{gb} (S/cm)	σ_t^t (S/cm)	E_a^g (eV)	E_a^{gb} (eV)	E_a^t (eV)(250–600 °C)	E_a^t (eV)(≥ 450 °C)
CSY0	0.65	6.5×10^{-3}	4.2×10^{-3}	2.7×10^{-3}	0.58	0.61	0.60	0.55
CSY5	0.61	8.0×10^{-3}	5.1×10^{-3}	3.1×10^{-3}	0.55	0.60	0.58	0.51
CSY10	0.43	2.0×10^{-2}	2.7×10^{-2}	1.1×10^{-2}	0.49	0.54	0.50	0.45
CSY15	0.49	9.7×10^{-3}	8.9×10^{-3}	4.4×10^{-3}	0.53	0.58	0.55	0.48
CSY20	0.51	8.4×10^{-3}	7.5×10^{-3}	3.9×10^{-3}	0.54	0.59	0.56	0.50
CSY10C	0.45	1.3×10^{-2}	1.5×10^{-2}	6.9×10^{-3}	0.51	0.56	0.52	0.46

Table 6 Comparison of total ionic conductivity (σ_t) with some studied systems

Composition	Sintering	Sintering temperature (°C)	σ_t (S/cm) at 500 °C	σ_t (S/cm) at 600 °C	Reference
Ce _{0.8} Sm _{0.1} Y _{0.1} O _{2-δ}	Microwave	1200	0.011	0.025	Present work
Ce _{0.8} Sm _{0.1} Y _{0.1} O _{2-δ}	Conventional	1300	0.0069	0.017	Present work
Ce _{0.85} La _{0.125} Sr _{0.025} O _{1.9}	Conventional	1350	–	0.015	[9]
Ce _{0.8} Sm _{0.1} Y _{0.1} O _{1.9}	Conventional	1500	–	0.036	[12]
Ce _{0.8} Sm _{0.1} Y _{0.1} O _{1.9}	Conventional	1300	–	0.013	[16]
Ce _{0.8} Sm _{0.18} Ca _{0.02} O _{2-δ}	Microwave	1450	0.0018	–	[19]
Ce _{1-x} Bi _x O _{2-δ}	Microwave	1050	–	0.0002	[20]
Ce _{0.83} Dy _{0.14} Ca _{0.03} O _{1.90}	Conventional	1350	–	0.014	[33]

and total ionic conductivity were calculated and presented in Table 5. The presence of attractive interactions between the trivalent dopant cations and presence of oxygen vacancies in ceria lattice result in migration of oxygen vacancies, which leads to lower activation energy. It can be seen that the microwave-sintered CSY10 sample shows lower activation energy than conventionally sintered CSY10C sample. The migration of oxygen vacancies results in small value of activation energy and enhances the total ionic conductivity of co-doped ceria [4–8, 31, 32]. Further, high doping levels of yttrium lowers interaction between oxygen vacancies and dopant cations which reduces the mobility of oxygen vacancies [34]. This, in turn, results in an increase in the activation energy and a decrease in the total ionic conductivity of ceria.

Thermal expansion

The thermal expansion of a material plays a key role for the applications of SOFC. Electrolyte materials must have equal thermal expansion coefficient (TEC) values with the electrodes to avoid micro-cracks between the adjacent cell components of SOFC at operating temperature [35–37]. The thermal expansion characteristic measurements (dL/L_0) of CSY system were determined in the temperature range from room temperature to 1000 °C. The thermal expansion coefficients were calculated from the thermal

expansion curves shown in Fig. 9. The following equation is used to calculate the thermal expansion coefficient for all the co-doped ceria specimens:

$$\text{TEC} = \frac{(L-L_0)/L_0}{T-T_0} \quad (5)$$

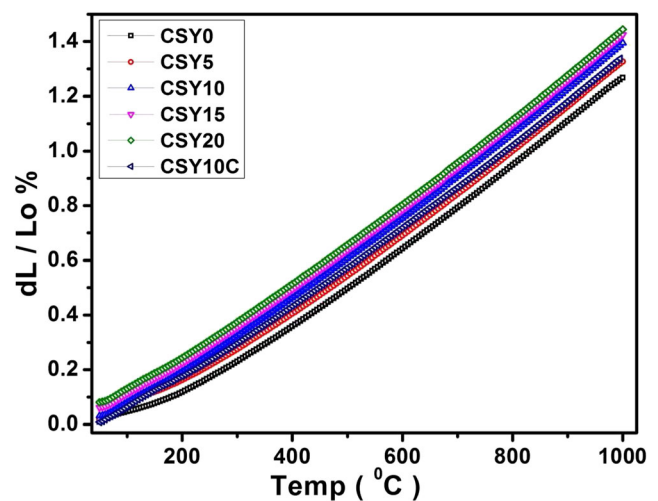
**Fig. 9** Thermal expansion curves with temperature variation of CSY system

Table 7 Thermal expansion coefficient (TEC) of CSY system

Sample	TEC ($\times 10^{-6}/^{\circ}\text{C}$)		
	RT–600 $^{\circ}\text{C}$	RT–800 $^{\circ}\text{C}$	RT–1000 $^{\circ}\text{C}$
CSY0	11.22	12.30	13.05
CSY5	11.64	12.69	13.42
CSY10	12.20	13.11	13.77
CSY15	12.55	13.39	13.99
CSY20	12.95	13.62	14.21
CSY10C	11.89	12.94	13.58

where L_0 is the initial length, L is the final length of a specimen, and T_0 and T are the starting and terminal temperatures for the experiment, respectively. The lattice thermal expansion curves were found to increase with the increase in temperature in the co-doped ceria oxide materials. It can be observed from Table 7 that the increase in yttrium concentration resulted in the increase of the TEC values. The concentration of the positive and negative charges and distance between them in the lattice (electrostatic forces) can influence the thermal expansion of a material. The TEC values also depend upon the attractive forces acting on the lattice. If attractive force decreases, it leads to a change in the lattice parameter values and increase in the thermal expansion of the material. This increase in the TEC values was accompanied by decreasing the unit cell parameters. This increment of TEC may be due to the loss of lattice oxygen or formation of lattice defects [32, 36]. The calculated TEC value for microwave-sintered CSY10 sample studied in the present investigation was found to be 13.77, which is close to TEC values of recently studied anode and cathode materials $\text{La}_{0.6}\text{Sr}_{1.4}\text{MnO}_4$ with 14.15 [38], $\text{La}_{2-x}\text{Pr}_x\text{NiO}_{4+\delta}$ material with 13.50 [39], and $\text{Ba}_{0.6}\text{Sr}_{0.4}\text{Co}_{0.9}\text{Nb}_{0.1}\text{O}_{3-\delta}$ –(20%) $\text{Gd}_{0.1}\text{Ce}_{0.9}\text{O}_{1.95}$ with 14.90 [40]. Therefore, it can be concluded that the TEC values of these Y^{3+} and Sm^{3+} co-doped ceria electrolytes were in good agreement and compatibility with the recently existing anode and cathode materials which make this material as suitable electrolyte for SOFC application.

Conclusion

The nanocrystalline, single-phase yttrium and samarium co-doped ceria solid electrolytes $\text{Ce}_{0.8}\text{Sm}_{0.2-x}\text{Y}_x\text{O}_{2-\delta}$ ($x = 0, 0.05, 0.1, 0.15, \text{ and } 0.20$) were successfully synthesized by sol–gel auto-combustion method followed by microwave sintering. Solid materials with high relative density were obtained by sintering the specimens at 1200 $^{\circ}\text{C}$ for 1 h using microwave and at 1300 $^{\circ}\text{C}$ for 4 h using conventional sintering. Single-phase pure cubic crystalline nature of samples was confirmed by X-ray diffraction analysis and the lattice parameters of the

unit cell were found to decrease linearly with increasing yttrium content. The micrographs of sintered samples with distribution of grains and elemental-composition analysis were confirmed by SEM and EDS analysis. The FTIR spectra of these co-doped ceria signifying the characteristic vibration frequency of metal oxygen bonds indicate the material formation. The presence of oxygen vacancies and evaluation of their concentration in the material was carried out using Raman analysis. The high value of concentrated oxygen vacancies in the microwave-sintered CSY10 sample with high relative density resulted in higher total ionic conductivity, i.e., 2.5×10^{-2} S/cm at 600 $^{\circ}\text{C}$ with lowest activation energy 0.50 eV. The microwave-sintered sample CSY10 at lower sintering temperature with less sintering time was found to have enhanced properties over conventional sintered CSY10C sample at higher sintering temperature with longer sintering time. Therefore, microwave-sintered CSY10, i.e., $\text{Ce}_{0.8}\text{Sm}_{0.1}\text{Y}_{0.1}\text{O}_{2-\delta}$, sample with high conductivity and thermal compatibility makes it useful as a promising electrolyte material in IT-SOFCs.

Acknowledgements One of the authors, K.V., thanks the University Grants Commission (UGC), New Delhi, India, for the financial assistance under the scheme of UGC-UPE-FAR program.

References

- Inaba H, Tagawa H (1996) Ceria-based solid electrolytes. *Solid State Ionics* 83:1–16. [https://doi.org/10.1016/0167-2738\(95\)00229-4](https://doi.org/10.1016/0167-2738(95)00229-4)
- Minh NQ (1993) Ceramic fuel cells. *J Am Ceramic Society* 76: 563–588. <https://doi.org/10.1111/j.1151-2916.1993.tb03645.x>
- Choy K, Bai W, Charojrochkul JS, Steele BCH (1998) The development of intermediate-temperature solid oxide fuel cells for the next millennium. *J Power Sources* 71:361–369. [https://doi.org/10.1016/S0378-7753\(97\)02728-6](https://doi.org/10.1016/S0378-7753(97)02728-6)
- Ramesh S, James Raju KC (2012) Preparation and characterization of $\text{Ce}_{1-x}(\text{Gd}_{0.5}\text{Pr}_{0.5})_x\text{O}_2$ electrolyte for IT-SOFCs. *Int J Hydrog Energy* 37:10311–10317. <https://doi.org/10.1016/j.ijhydene.2012.04.008>
- Stojmenovic M, Zunic M, Gulicovski J, B-Bogdanovic D, H-Antunovic I, Dodevskti V, Mentus S (2015) Structural, morphological, and electrical properties of doped ceria as a solid electrolyte for intermediate-temperature solid oxide fuel cells. *J Mater Sci* 50: 3781–3794. <https://doi.org/10.1007/s10853-015-8943-y>
- Khakpour Z, Youzbashi AA, Maghsoudipour A (2014) Influence of Gd^{3+} and Dy^{3+} co-doping and sintering regime on enhancement of electrical conductivity of ceria-based solid electrolyte. *Ionics* 20: 1407–1417. <https://doi.org/10.1007/s11581-014-1090-7>
- Fu Y-P, Chen S-H, Huang J-J (2010) Preparation and characterization of $\text{Ce}_{0.8}\text{M}_{0.2}\text{O}_{2-\delta}$ ($M = \text{Y, Gd, Sm, Nd, La}$) solid electrolyte materials for solid oxide fuel cells. *Int J Hydrog Energy* 35:745–752. <https://doi.org/10.1016/j.ijhydene.2009.10.093>
- Pikalova EY, Murashkina AA, Maragou VI, Demin AK, Strekalovsky VN, Tsiakaras PE (2011) CeO_2 based materials doped with lanthanides for applications in intermediate temperature electrochemical devices. *Int J Hydrog Energy* 36:6175–6183. <https://doi.org/10.1016/j.ijhydene.2011.01.132>
- Jaiswal N, Kumar D, Upadhyay S, Parkash O (2015) Preparation and characterization of $\text{Ce}_{0.85}\text{La}_{0.15-x}\text{Sr}_x\text{O}_{\{2-(0.075+x/2)\}}$ solid

- electrolytes for intermediate temperature solid oxide fuel cells. *Ionics* 21:497–505. <https://doi.org/10.1007/s11581-014-1190-4>
10. Padmasree KP, M-Lozano RA, Montemayor SM, Fuentes AF (2011) Electrical conduction and dielectric relaxation process in $\text{Ce}_{0.8}\text{Y}_{0.2}\text{O}_{1.9}$ electrolyte system. *J of Alloys and Compounds* 509:8584–8589. <https://doi.org/10.1016/j.jallcom.2011.06.036>
 11. BifaJi CT, Wang C, Tong W, JinsongXie ML (2015) Preparation and characterization of $\text{Ce}_{0.8}\text{Y}_{0.2-x}\text{Cu}_x\text{O}_{2-\delta}$ as electrolyte for intermediate temperature solid oxide fuel cells. *J Power Sources* 278:420–429. <https://doi.org/10.1016/j.jpowsour.2014.12.073>
 12. Dudek M, Bogusz W, Zych L, Trybalska B (2008) Electrical and mechanical properties of CeO_2 -based electrolytes in the CeO_2 - Sm_2O_3 - M_2O_3 (M = La, Y) system. *Solid State Ionics* 179:164–167. <https://doi.org/10.1016/j.ssi.2007.12.023>
 13. Dudek M, Mroz M, Zych L, D-Ciesla E (2008) Synthesis of ceria-based nano powders suitable for manufacturing solid oxide fuel cells. *Materials Science-Poland* 26(2):319–330. 10.11498.7080
 14. Dudek M (2008) Ceramic oxide electrolytes based on CeO_2 —preparation, properties and possibility of application to electrochemical devices. *J European Ceramic Society* 28:965–971. <https://doi.org/10.1016/j.jeurceramsoc.2007.09.004>
 15. Cheng J, Jiang Q, He H, Yang J, Wang Y, Gao J (2011) Preparation and characterization of Y_2O_3 - Sm_2O_3 co-doped ceria electrolyte for IT-SOFCs. *Mater Chem Phys* 125:704–708. <https://doi.org/10.1016/j.matchemphys.2010.09.070>
 16. Sha X, Lu Z, Haung X, Miao J, Liu Z, Xin X, Zhang Y, Su W (2007) Influence of the sintering temperature on electrical property of the $\text{Ce}_{0.8}\text{Sm}_{0.1}\text{Y}_{0.1}\text{O}_{1.9}$ electrolyte. *J. Alloys and Compounds* 433:274–278. <https://doi.org/10.1016/j.jallcom.2006.06.062>
 17. Oghbaei M, Mirzaee O (2010) Microwave versus conventional sintering: a review of fundamentals, advantages and applications. *J. Alloys and Compounds* 494:175–189. <https://doi.org/10.1016/j.jallcom.2010.01.068>
 18. Chockalingam R, Chockalingam S, Vasantha RW, Amarakoon (2011) The electrical properties of microwave sintered gadolinia doped ceria-alumina nano-composite electrolyte. *J Power Sources* 196:1808–1817. <https://doi.org/10.1016/j.jpowsour.2010.09.074>
 19. P-Gonjal J, Heuguet R, M-Gil D, R-Calzada A, Marinel S, Moran E, Schmidt R (2015) Microwave synthesis & sintering of Sm and Ca co-doped ceria ceramics. *Int J Hydrog Energy* 40:15640–15651. <https://doi.org/10.1016/j.ijhydene.2015.07.161>
 20. Prekajski M, Stojmenovic M, Radojkovic A, Brankovic G, Oraon H, Subasri R, Matovic B (2014) Sintering and electrical properties of $\text{Ce}_{1-x}\text{Bi}_x\text{O}_{2-\delta}$ solid solution. *J Alloys and Compounds* 617:563–568. <https://doi.org/10.1016/j.jallcom.2014.08.090>
 21. Shannon RP, Prewitt T (1969) Effective ionic radii in oxides and fluorides. *Acta Crystallogr B* 25:925–946. <https://doi.org/10.1107/S0567740869003220>
 22. Dikmen S, Aslanbay H, Dikmen E, Sahin O (2010) Hydrothermal preparation and electrochemical properties of Gd^{3+} and Bi^{3+} , Sm^{3+} , La^{3+} , and Nd^{3+} codoped ceria-based electrolytes for intermediate temperature-solid oxide fuel cell. *J Power Sources* 195:2488–2495. <https://doi.org/10.1016/j.jpowsour.2009.11.077>
 23. SubrataKundu NS, Thangamuthu R, Subramanian B, Panda AB, Jayachandran M (2012) Fabrication of catalytically active nanocrystalline samarium (Sm)-doped cerium oxide (CeO_2) thin films using electron beam evaporation. *J Nano part Res* 14:1040. <https://doi.org/10.1007/s11051-012-1040-0>
 24. Arumugam A, Karthikeyan C, Hameed ASH, Gopinath K, Gowri S, karthika V (2015) Synthesis of cerium oxide nanoparticles using *Gloriosa superba* L. leaf extract and their structural, optical and antibacterial properties. *Mater Sci Eng C* 49:408–415. <https://doi.org/10.1016/j.msec.2015.01.042>
 25. Bhabu KA, Theerthagiri J, Madhavan J, Balu T, Muralidharan G, Rajasekaran TR (2016) Cubic fluorite phase of samarium doped cerium oxide (CeO_2)_{0.96}Sm_{0.04} for solid oxide fuel cell electrolyte. *J Mater Sci Mater Electron* 27:1566–1573. <https://doi.org/10.1007/s10854-015-3925-z>
 26. Uslu I, ArdaAytimur M k, Serhatkocyigit (2012) Synthesis and characterization of neodymium doped ceria nanocrystalline ceramic structures. *Ceram Int* 38:4943–4951. <https://doi.org/10.1016/j.ceramint.2012.02.087>
 27. Wattanathana W, Nootsuwan N, Veranitisagul C, Koonsaeng N, Laosiripojana N, Laobuthee A (2015) Simple cerium-triethanolamine complex: synthesis, characterization, thermal decomposition and its application to prepare ceria support for platinum catalysts used in methane steam reforming. *J Mol Struct* 1089:9–15. <https://doi.org/10.1016/j.molstruc.2015.02.010>
 28. Limmer W, Ritter W, Sauer R (1998) Raman scattering in ion-implanted GaN. *Appl Phys Lett* 72:2589–2591. <https://doi.org/10.1063/1.121426>
 29. Mandal BP, Roy M, Grover V, Tyagi AK (2008) X-ray diffraction, μ -Raman spectroscopic studies on CeO_2 - RE_2O_3 (RE = Ho, Er) systems: observation of parasitic phases. *J. Appl. Phys* 103:33506-1–33506-7. <https://doi.org/10.1063/1.2837042>
 30. López JM, Gilbank AL, García T, Solsóna B, Agouram S, Torrente-Murciano L (2015) The prevalence of surface oxygen vacancies over the mobility of bulk oxygen nanostructured ceria for the total toluene oxidation. *Appl Catal B Environ* 174–175:403–412. <https://doi.org/10.1016/j.apcatb.2015.03.017>
 31. Li S-P, Lu J-Q, Fang P, Luo M-F (2009) Effect of oxygen vacancies on electrical properties of $\text{Ce}_{0.8}\text{Sm}_{0.1}\text{Nd}_{0.1}\text{O}_{2-\delta}$ electrolyte: an in situ Raman spectroscopic study. *J Power Sources* 193:93–98. <https://doi.org/10.1016/j.jpowsour.2008.12.022>
 32. Prashanth Kumar V, Reddy YS (2008) Thermal and electrical properties of rare-earth co-doped ceria ceramics. *Mater Chem Phys* 112:711–718. <https://doi.org/10.1016/j.matchemphys.2008.06.030>
 33. Tanwar K, Jaiswal N, Kumar D, Parkash O (2016) Synthesis & characterization of Dy and Ca co-doped ceria based solid electrolytes for IT-SOFCs. *J. Alloys and Compounds* 684:683–690. <https://doi.org/10.1016/j.jallcom.2016.05.223>
 34. Anderson DA, Simak SI, Skorodumova NV, Abrikosov IA, Johansson B (2006) Optimization of ionic conductivity in doped ceria. *PANS* 103:3518–3521. <https://doi.org/10.1073/pnas.0509537103>
 35. Venkataramana K, Madhuri C, Suresh Reddy Y, Bhikshamaiah G, Vishnuvardhan Reddy C (2017) Structural, electrical and thermal expansion studies of tri-doped ceria electrolyte materials for IT-SOFCs. *J. Alloys Compd* 719:97–107. <https://doi.org/10.1016/j.jalcom.2017.05.022>
 36. Ramesh S, Kumar VP, Kistaiah P, Reddy CV (2010) Preparation, characterization and thermo electrical properties of co-doped $\text{Ce}_{0.8-x}\text{Sm}_{0.2}\text{Ca}_x\text{O}_{2-\delta}$ materials. *Solid State Ionics* 181:86–91. <https://doi.org/10.1016/j.ssi.2009.11.014>
 37. Wu Y-C, Lin C-C (2014) The microstructures and property analysis of aliovalent cations (Sm^{3+} , Mg^{2+} , Ca^{2+} , Sr^{2+} , Ba^{2+}) co-doped ceria-based electrolytes after aging treatment. *Int J Hydrog Energy* 39:7988–8001. <https://doi.org/10.1016/j.ijhydene.2014.03.063>
 38. Jin C, Yang Z, Zhang H, Yang C, Chen F (2012) $\text{La}_{0.6}\text{Sr}_{1.4}\text{MnO}_4$ layered perovskite anode material for intermediate temperature solid oxide fuel cells. *Electrochemistry Commun* 14:75–77. <https://doi.org/10.1016/j.elecom.2011.11.008>
 39. VaibhavVibhu AR, Nicolle C, AurelienFlura J-CG, Bassat J-M (2015) $\text{La}_{2-x}\text{Pr}_x\text{NiO}_{4+\delta}$ as suitable cathodes for metal supported SOFCs. *Solid State Ionics* 278:32–37. <https://doi.org/10.1016/j.ssi.2015.05.005>
 40. Zhang L, Mo L, Huang J, Song Z (2014) Improved thermal expansion and electrochemical performances of $\text{Ba}_{0.6}\text{Sr}_{0.4}\text{Co}_{0.9}\text{Nb}_{0.1}\text{O}_{3-\delta}$ - $\text{Gd}_{0.1}\text{Ce}_{0.9}\text{O}_{1.95}$ composite cathodes for IT-SOFCs. *Int J Hydrog Energy* 39:7972–7979. <https://doi.org/10.1016/j.ijhydene.2014.03.055>